September 14, 2001, FTM2001-11, Version 2

Two Dimensional sinc^2 PSFs for FAME

Centroiding Precision along the Cross-Scan Diffraction Ridge

Rob Olling

USNO/USRA, Washington, DC

ABSTRACT

I present results of an analysis into the feasibility of centroiding bright stars on the cross-scan diffraction ridge. To first order, FAME's two-dimensional point-spread function (PSF) looks like the product of two sinc^2 functions. In the in-scan direction, the PSF falls off rapidly, whereas the decline in the cross-scan direction is slower by the ratio of the aperture dimensions, or 40/9=4.44 in the "current" FAME design. Broadly speaking, the achievable centroiding precision is determined by three factors: 1) The peak number of photo-electrons in the in-scan profile, 2) the full-width at half maximum (FWHM) of the PSF, and 3) the in-scan and cross-scan smearing.

The cross-scan intensity decrease is rather gradual beyond the first 5 pixels or so. For the "average" star I find that the peak in-scan intensity decreases by 0.0, 3.8, 4.8, 6.4, 7.2, 7.9 and 8.3 magnitudes at cross-scan positions of 0, 5, 10, 20, 30, 40 and 60 pixels, respectively.

To first order, the in-scan width of the cross-scan ridge is set by the long dimension of the mirror, and is hence invariant with respect to cross-scan position. Second order effects introduce color-dependent width variations, while optical distortions will further modify the detailed cross-scan variation of the in-scan PSF. The cross-scan variation of in-scan PSF width is determined by the spectral energy distribution (SED) of the target star, and is of order $\pm 6\%$, in both the wide and narrow astrometric band. At large cross-scan distances, the color-induced width variations decreases significantly.

Bright stars that would over-fill the CCD pixels spread the additional charge mostly in the in-scan direction (John Geary, private communications). If such bright stars are read-out in 2D mode, neither the serial wells, nor the summing wells will overflow. As a result, practically all columns that do not exceed the full-well capacity in their brightest pixels can be used for centroiding/photometry. Astrometry and photometry of such bright stars would be most profitably done

on 2D postage stamps that extend sufficiently in the cross-scan direction to reach the linear part of the CCD response curve. In particular, it is expected that data on both sides of the cross-scan diffraction ridges can greatly aid the determination of the optical distortions (Murison, private communications).

Due to the column-multiplexing, the achievable centroiding precision *per raster* is very good for the bright stars. With a lower limit to the centroiding precision of $1/350^{th}$ of a pixel per column in the 2D raster, centroiding errors of 80 μas at V=1 and 340 μas at V=9, *per transit* can be achieved. There also exists a slight multiplexing advantage for cross-scan positioning.

Large 2D postage stamps are also needed for the photometric calibration of the astrometric and photometric bandpasses: about 60 mmag (6%) of the flux is missing in a window of 13x25 pixels. An analytic expression is given that describes the the aperture-photometry function to acceptable accuracy. Finally it may be profitable to increase the in-scan length of the FAME postage stamp by several pixels (2-4) so as to be able to adequately centroid/photometer in the presence of a (sloping) background (e.g. due to stray-light from the Earth or Moon). This has to be traded with the available data and star transit rates.

1. Introduction

Two-dimensional PSFs are created assuming that the PSF in both in-scan and cross-scan directions are poly-chromatic sinc^2 functions. At a given wavelength, the intensity profile is given by:

$$I(x,y;\lambda) = A(T_{eff},QE,TP)\,\mathrm{sinc}^2(x)\,\mathrm{sinc}^2(y) \quad (1)$$

where

$$x(\lambda) = \phi_x + \frac{\pi\, u\, D_x\, d_{pix}}{F\,\lambda} \quad (2)$$

$$y(\lambda) = \phi_y + \frac{\pi\, v\, D_y\, d_{pix}}{F\,\lambda} \quad (3)$$

where $\phi_{x,y}$ is the pixel phase in direction x or y, u and v are distances expressed in units of pixels, D_x and D_y are the diameters of the mirror in the x and y directions, d_{pix} the pixel size, F the focal length, and λ the wavelength. The scale-factor $A(\lambda;T_{eff},QE,TP)$ depends on the stellar SED (T_{eff}), the quantum efficiency of the CCD (QE) and the throughput (TP) of the optical system. Polychromatic PSFs are created by summing $I(x;\lambda)$ for discrete sub-pixel locations (30) and by binning $A(\lambda;T_{eff},QE,TP)$ in steps of 22 nm.

2. Results

2.1. 2D PSFs

In figure 1, I present 2D PSFs for six models at three temperatures (Vega/9400K, Sun/5777, 3500K) and two astrometric bandpasses (400-900 and 550-850 nm). The $x-$ and y-axes represent the in- and cross-scan directions. All images are for zero pixel-phase and are integrated over the pixels. The contours are determined with respect to the peak flux, and are drawn at 1 magnitude intervals (lowest contour is at -10 mag). It is clearly visible that the in-scan width is substantially larger than the cross-scan width and that the in-scan width varies with cross-scan location. Also note that the low-temperature models (top panels) appear more "wavy" due to the fact that their SEDs peak much more strongly than Solar-type or Vega-like stars. As a result, as compared to hotter stars, there is less wavelength smearing of the $\mathrm{sinc}^2(\lambda)$ components, so that the low-T_{eff} poly-chromatic PSFs are more mono-chromatic. Comparing the wide and narrow astrometric bands in the left- and right-hand panels, we notice a similar effect. The narrow band PSFs show a more pronounced "ringing" due to the fact that it is more "mono-chromatic" than the wide astrometric band: that is to say, there is less wavelenght-induced smearing. And finally, the same effect can be been seen in the cross-scan intensity profiles displayed in the top panels of figures 2-4.

For 2D images, the dynamic range equals 14 bits, or a factor of 16,384 (10.5 magnitudes), so that the lowest contour (-10 mag) corresponds roughly to the lowest ADU values returned (1 ADU, or $100k/16k \sim 6$ e$^-$). If the readnoise equals 30 e$^-$ per pixel, the lowest two to three contours will disappear in the noise if no further re-binning is applied in the data analysis.

2.2. Cross-Scan Variation of the In-Scan PSF

In figures 2-4, I present the cross-scan variation of: 1) the peak of the in-scan PSF (top panel), 2) the full width at half maximum (FWHM) of the in-scan PSF derived from a Gaussian fit (middle panel), and 3) (bottom panel) the estimated achievable precisions for the centroid (black line), FWHM (red line) and total flux (green line). From previous experimentations (unpublished) with FAMEx0.7 PSFs, I find the following fit-precisions for the centroiding, widths and total flux:

$$\frac{\delta x_0}{x_0} \sim 100 \times \left(0.000 + \frac{0.5443}{N} + \frac{13.44}{N^2}\right) \left(\frac{FWHM}{1.99}\right)^{1.5} \% \quad (4)$$

$$\frac{\delta FWHM}{FWHM} \sim 100 \times \left(0.000 + \frac{0.3471}{N} + \frac{37.70}{N^2}\right) \% \quad (5)$$

$$\frac{\delta Flux}{Flux} \sim 10 \times \left(0.546 + \frac{858}{N} + \frac{18,879}{N^2}\right) \% \quad (6)$$

where N is the square-root of the total flux in the 1D, 13-pixel in-scan box.

For typical stars, the peak in-scan intensity decreases by 0.0, 3.8, 4.8, 6.4, 7.2, 7.9 and 8.3 magnitudes at cross-scan positions of 0, 5, 10, 20, 30, 40 and 60 pixels, respectively. Note that in-scan and cross-scan smearing *does* reduce the peak flux in 2D images: a factor of two reduction in peak flux occurs when the stellar images is smeared by a pill-box that has a width equal to approximately twice the FWHM of the optical PSF ($\sim$2 pixels in the in-scan and $\sim$8 pixels in the cross-scan direction).

In the middle plot of each panel of figures 2-4, I also list the minimum, average and maximum values of the $FWHM$ of the in-scan PSFs, as well as the maximum fractional variation (Δ/AVE). The average widths are clearly a strong function of T_{eff}: $FWHM = 1.32, 1.27$ and 1.24 for T_{eff}= 3,500, 5,777 and 9,400 Kelvin for the narrow bandpass. Since $FWHM \propto \lambda_{eff}/D$, the change in $FWHM$ can be interpreted as a change in effective wavelength. Also note that the amplitude of the $FWHM$ variation changes with cross-scan position, and that the variation for hot stars damps out more rapidly with cross-scan distance.

2.2.1. Unsaturated Stars

In figures 2-4, the top row of figures is for the case that the full-well capacity is reached (100k electrons) in the central pixel of the 2D image. These sets of figures illustrate what can be learned from unsaturated 2D imaged, and to what precisions. Comparing the three figures, we see that the cross-scan variation of the in-scan FWHM is a function of the effective SED. Out to $\pm$10 pixels it varies by about $\pm$7 %, whereas the widths can be measured is better than 2%.

For barely unsaturated images, the centroid can be determined to $\pm 1/350^{th}$ of a pixel ($\sim$ 0.4%) for the 6 brightest columns. However, the centroiding *bias* may be ten times larger than the centroiding precision, or up to 4% of the width of a pixel. Figures 2-4 show that such a 4% bias can be determined at the $\lesssim 2\sigma$ level out to about $\pm$10 pixels. Of course, the data in the low-amplitude parts of the cross-scan wings may be smoothed to further improve the centroiding.

2.2.2. Saturated Stars

In figures 2-4, the bottom row is for the case that the target star is 5 magnitudes brighter and yield 100 times more photo electrons in the peak. These plots have a larger range in cross-scan position. From these figures it follows that a star of magnitude 4 would no longer

saturate the CCD at cross-scan distances larger than ∼10 pixels[1]. Because the cross-scan intensity fall off is relatively slow at large distances, many columns contain enough flux to achieve 0.4% centroiding precision: about 15 pixels on either side for the case presented here. Again, a larger part of the diffraction ridge may be used to further improve the results.

At a cross-scan distance of 65 columns, the achievable attenuation equals about 9 magnitudes. In principle, there is no limit to the cross-scan extent of the postage stamps, so that *all* stars can measured. Since there exist very few bright stars[2], the impact on the data rate is small. If we assume that all stars brighter than V=6 will be done with a 130x13 postage stamp and all stars with $6 \leq V \leq 9$ with a 40x13 raster, the additional data comprises just twice the amount as would be the case for "standard" 24x13 postage stamps.

2.3. CCD Effects

A problem with saturating the CCD in certain pixels is that the excess charge has to go somewhere. However, it is expected that "blooming" will occur in the in-scan direction, and that hardly any charge will spill over in the cross-scan direction (John Geary, private communications). Furthermore, because of the blooming, no 2D pixels will contains significantly more than 100k electrons. As a result, neither the serial well nor the summing wells will saturate when a saturated star arrives at end of a column. Thus, neither the cross-scan ridge closest to the amplifier, nor the far side will be significantly affected by charge overflow, especially since we can easily move several columns further outwards.

2.4. 2D Raster Spin-Offs

Since CCD effects will hardly corrupt the diffraction ridges a few columns away from the saturated columns, large parts of the 2D image are available for centroiding analysis. This effect can be exploited to calibrate instrumental effects such as the optical distortions or more mundane effects such as the tilt of the CCD with respect to the scan direction.

In table 2, I report the precision to which the CCD orientation can be determined. The achievable in-scan and cross-scan centroiding precisions per 2D raster is determined as: $\overline{\delta x_0} = \sqrt{1/\sum_c 1/(\delta x_0(c))^2}$, with $\delta x_0(c)$ the precision in each un-saturated column. Due to the column-multiplexing, the achievable centroiding precision *per raster* is quite small for the bright stars.

---

[1] Assuming that a V=9 star yields a peak flux of 100k photo-electrons.

[2] There are just 4,239 stars with $m_V \leq 6.0$ and 41,485 stars with $m_V \leq 8.0$ in the Tycho catalog.

The results reported here are determined for rasters of size up to 255x255 pixels. However, only unsaturated columns and rows were used. Furthermore, the smallest contiguous region with signal-to-noise ratios (S/N) between 3 and 6 were binned together to improve the centroiding precision[3]. Regions with peak S/N below 3 were discarded altogether. In the second column of table 2, I list the number of columns of the cross-scan diffraction ridge ($N_{C,f}$) that was used in the fit. The 3^{rd} column lists the minimum box size in the cross-scan direction ($N_{C,b}$). For the determination of the cross-scan precision, only the rows in the leading in-scan diffraction ridge were used: their number ($N_{I,f}$) is listed in column # 9, while the corresponding minimum in-scan box size ($N_{I,b}$) is listed in the 10^{th} column.

In the 4^{th} column, I tabulate the precision with which the orientation of the CCD with respect to the scan direction can be determined: 0.46, 1.05, 3.13, 9.19, and 24.6 arcseconds *per transit* for stars with magnitudes V=1, 3, 5, 7 and 9, respectively.

In the 5^{th} column, I tabulate photon-statistics limit to the in-scan centroiding precision. The 7^{th} column tabulates the in-scan centroiding precision for the case that each individual measurement is limited to a precision of $1/350^{th}$ of a pixel. I find: 72, 88, 135, 226, 293 and 514 μas at V=1, 3, 5, 7, 9 and 11 *per transit*.

Finally, in the last column, I list the precision to which the cross-scan position can be determined, per transit. I find: 0.73, 1.19, 1.70, 3.41, 2.43 and 6.78 at V=1, 3, 5, 7 and 9, respectively.

3. Photometry With FAME

FAME Photometry is required for both the astrometric and photometric passbands. At V=9, the achievable precision in the (descoped) narrow astrometric band is about 2 mmag per transit, 3 mmag for an SDSS band and 5 mmag for the 50-nm Astrophysical bands. Thus, the total per-transit number of photons can be measured with a 1σ error 0.2% to 0.5%. The sytematic errors are likely to be much larger. One source of systematic error arises from the fact that some photons land outside the FAME postage stamp (13x24 pixels).

With the aid of large 2D sinc^2 PSFs it is possible to estimate how much of the total stellar flux is lost. For this purpose, I assume that 100% of the flux is contained in 2D images of size 130x130 pixels. This assumption is certainly not true, but adequate to estimate how much flux is lost in the standard 13x24 pixels. Furthermore, it is possible to investigate how much the lost-flux fraction depends on 1) window size, 2) TDI-rate mismatch, and 3)

[3]This is worthwhile because the precision decreases faster than photon statistics at low flux levels.

Table 1: As a function of visual magnitude (1^{th} column), I present the precision to which the orientation of the CCD can be determined (5^{rd}) and the centroiding precision in units of milli-arcseconds (6^{th}) and fractions of a pixel (7^{th}). The δx_0 values in columns #8 and #9 assume a lower bound to the centroiding precision of $1/350^{th}$ of a pixel, per column. The cross-scan raster size equals **256** pixels. Only unsaturated columns, in the ranges $[-C_U, -C_L]$ and $[C_L, C_U]$, are used in the centroiding experiment. Some columns are averaged to enhance the signal-to-noise ration. The total number of valid columns listed in #4. The last two columns enumerate the maximum and minimum peak values in unsaturated image. The readnoise is taken to be 30 e^- per pixel.

m_V	$\mid C_L \mid$	$\mid C_U \mid$	N_{VAL}	$\sigma_{CCD-ori}$ [arcsec]	δx_0 [mas]	δx_0 [1/pixel]	δx_0^{bias} [mas]	δx_0^{bias} [1/pixel]	MAX e^-	MIN e^-
(1)	(2)	(3)	(4)	(5)	(6)	(7)	(8)	(9)	(10)	(11)
0.0	54	127	108	0.346	0.047	6246	0.082	3595	98.16	12.40
1.0	36	127	158	0.457	0.051	5745	0.072	4082	95.57	4.94
2.0	27	127	194	0.663	0.057	5136	0.076	3880	98.99	1.97
3.0	17	127	218	1.050	0.069	4291	0.088	3335	85.67	0.78
4.0	11	127	234	1.731	0.079	3710	0.105	2804	92.98	0.31
5.0	5	112	208	3.150	0.111	2643	0.135	2181	70.69	0.22
6.0	4	127	228	5.363	0.129	2279	0.163	1808	71.64	0.13
7.0	4	126	180	9.551	0.220	1340	0.227	1297	28.52	0.14
8.0	3	106	116	16.927	0.271	1085	0.322	915	46.98	0.14
9.0	0	98	83	27.121	0.181	1622	0.293	1004	100.00	0.15
10.0	0	50	51	62.793	0.303	972	0.352	835	39.81	0.14
11.0	0	21	31	156.098	0.517	570	0.517	570	15.85	0.13
12.0	0	11	17	349.698	0.907	325	0.907	325	6.31	0.18

cross-scan smearing.

In figure 5, I present the amount of missing flux as a function of in-scan and cross-scan box size. The contours are labeled in units of mmag (∼0.1%). The amount of missing flux exceeds the achievable precision for all box sizes considered, and for the 13x24 window, about 6% falls *outside* the box. In practice, this amount may be estimated by aperture photometry. In this technique, the amount of flux is plotted as a function of aperture size, and extrapolated to infinite radius. Given the large amount of missing flux (6%) and the high precision required (0.2%), it is important to be able to calibrate the missing flux curve on images that are significantly larger than the standard size. Such large images would have to be scheduled regularly. Because of the cross-shaped 2D PSF, aperture photometry will extend preferentially along the in-scan and cross-scan directions, and avoid/down-weight the intermediate regions.

Table 2: Same as table 1 but for a cross-scan raster size of 128 pixels.

m_V	$\mid C_L \mid$	$\mid C_U \mid$	N_{VAL}	$\sigma_{CCD-ori}$ [arcsec]	δx_0 [mas]	δx_0 [1/pixel]	δx_0^{bias} [mas]	δx_0^{bias} [1/pixel]	MAX e^-	MIN e^-
(1)	(2)	(3)	(4)	(5)	(6)	(7)	(8)	(9)	(10)	(11)
0.0	54	63	6	2.56	0.215	1367	0.343	857	93.54	23.33
1.0	36	63	30	1.16	0.087	3388	0.159	1847	95.57	9.29
2.0	27	63	66	1.09	0.068	4333	0.107	2739	98.99	3.70
3.0	17	63	90	1.51	0.074	3983	0.100	2930	85.67	1.47
4.0	11	63	106	2.30	0.082	3602	0.111	2659	92.98	0.59
5.0	5	63	112	3.87	0.113	2604	0.138	2133	70.69	0.23
6.0	4	58	108	6.65	0.130	2263	0.165	1788	71.64	0.41
7.0	4	58	108	12.05	0.221	1332	0.228	1288	28.52	0.16
8.0	3	62	100	21.04	0.272	1081	0.323	911	46.98	0.14
9.0	0	56	79	36.65	0.182	1620	0.294	1002	100.00	0.15
10.0	0	50	51	62.79	0.303	972	0.352	835	39.81	0.14
11.0	0	21	31	156.10	0.517	570	0.517	570	15.85	0.13
12.0	0	11	17	349.70	0.907	325	0.907	325	6.31	0.18

At this point, no *firm* estimate of the required box size can be made. However, above we have seen that the PSF has declined by 9 magnitudes (factor 4,000) at a distance of 65 cross-scan pixels from the peak. For not-quite saturated stars, the intensity on the cross-scan ridge would thus be 25 e^-, which is comparable to the readnoise of 30 e^-. Since readnoise averages out, the aperture-photometry box can be profitably increased to *at least* 130 pixels in the cross-scan direction (and 130/4=16 pixels in the in-scan direction). If worse comes to worse, it would be possible to schedule adjacent 2D rasters to simulate the large 2D calibration images. However, the scheduling of adjacent rasters may be harder than scheduling a single large box.

The missing flux in the FAME 13x24 window depends on the stellar SED and the in-scan and cross-scan smearing. I have performed aperture photometry on models with the three T_{eff} values above and varied the smearings. The results are encouraging, as displayed in figure 6: for a given T_{eff}, the missing flux hardly changes with TDI-mismatch and cross-scan smearing. Only for very large values values does the variation in the missing flux exceed the single-transit precision. Furthermore, the dependence of the missing flux on the parameters considered is smooth, and it is expected that it can be well established (in software).

Table 3: Same as table 1 but for a cross-scan raster size of 60 pixels.

m_V	$\mid C_L \mid$	$\mid C_U \mid$	N_{VAL}	$\sigma_{CCD-ori}$ [arcsec]	δx_0 [mas]	δx_0 [1/pixel]	δx_0^{bias} [mas]	δx_0^{bias} [1/pixel]	MAX e^-	MIN e^-
(1)	(2)	(3)	(4)	(5)	(6)	(7)	(8)	(9)	(10)	(11)
2.0	27	29	2	—	0.258	1141	0.595	495	98.99	98.99
3.0	17	29	22	3.039	0.102	2897	0.179	1642	85.67	39.41
4.0	11	29	38	3.618	0.091	3222	0.139	2117	92.98	15.69
5.0	5	29	44	5.714	0.121	2436	0.153	1925	70.69	6.24
6.0	4	29	52	8.779	0.133	2208	0.171	1719	71.64	2.49
7.0	4	29	52	15.329	0.225	1306	0.233	1262	28.52	0.99
8.0	3	29	54	26.479	0.274	1072	0.327	900	46.98	0.39
9.0	0	29	59	45.176	0.182	1618	0.295	999	100.00	0.16
10.0	0	29	47	80.881	0.303	970	0.353	834	39.81	0.14
11.0	0	21	31	156.098	0.517	570	0.517	570	15.85	0.13
12.0	0	11	17	349.698	0.907	325	0.907	325	6.31	0.18

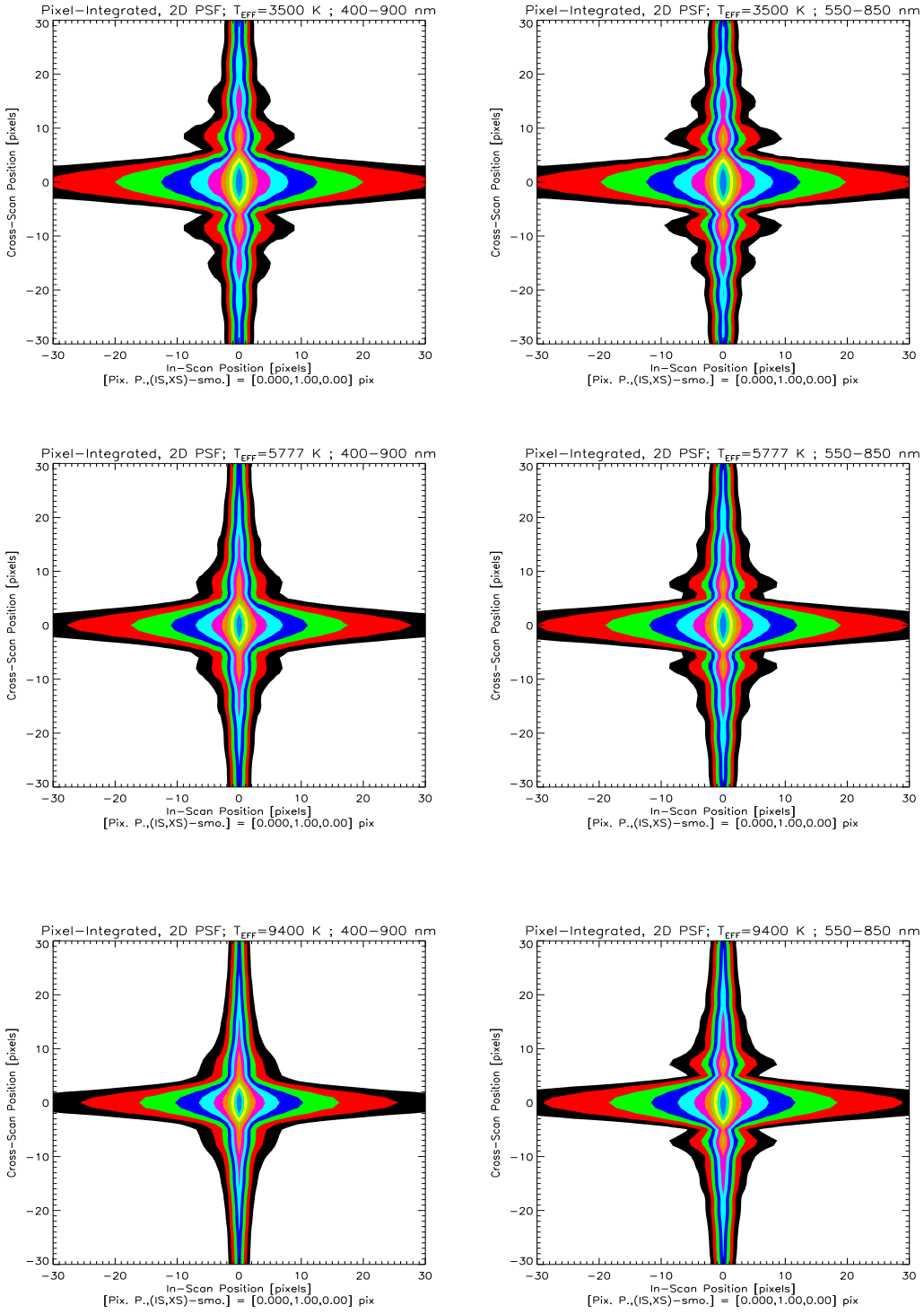

Fig. 1.— The 2D sinc^2 PSFs for stars with T_{eff} = 3500K, 5777K and 9400K for the wide bandpass (left panels) and the narrow bandpass (right panels). The color contours represent the attenuation with respect to the peak, at an interval of 1 magnitude (lowest contour is at -10 magnitudes).

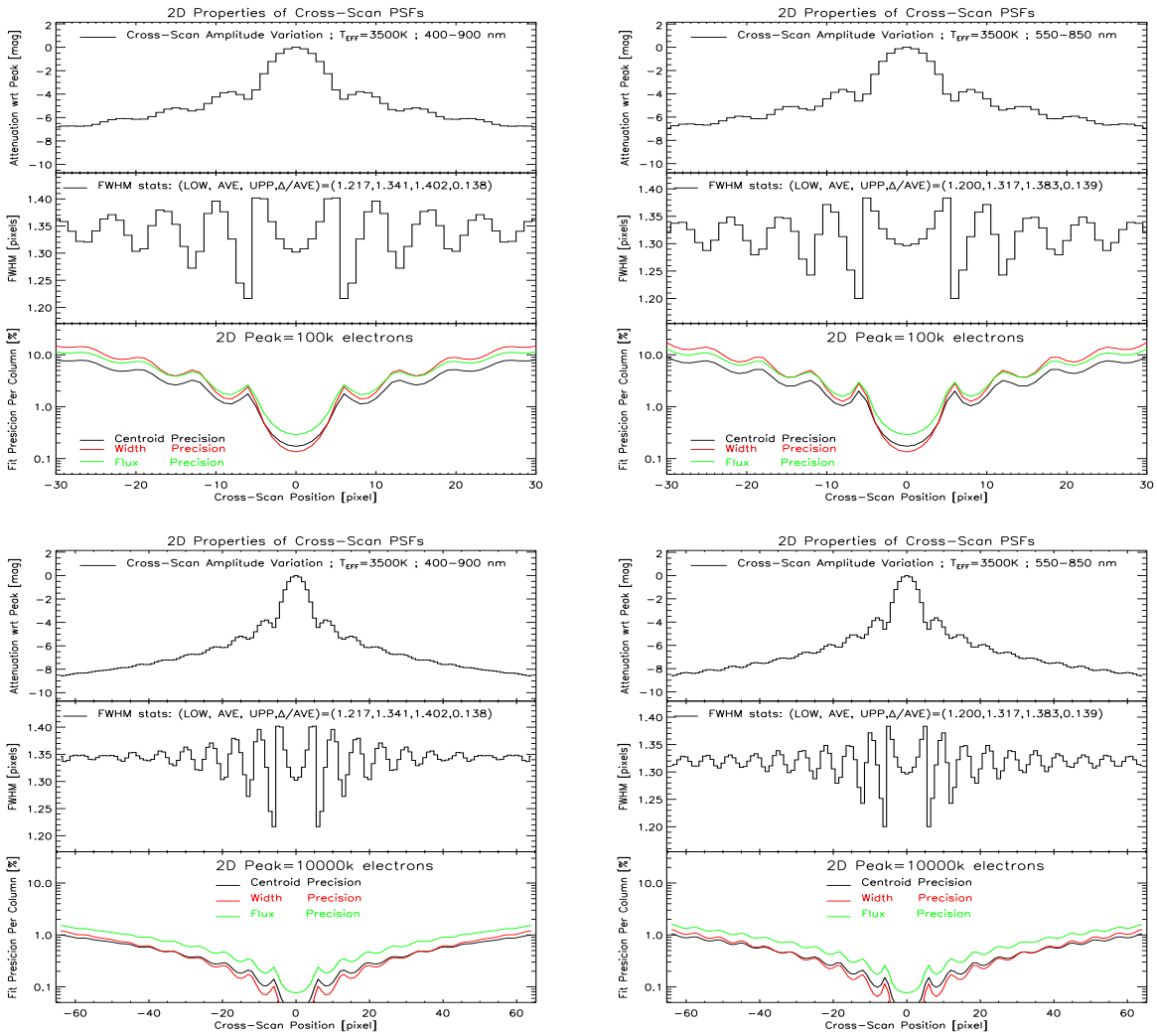

Fig. 2.— In each of the four figures of this collage, I present (in the top, middle and bottom panels) the cross-scan variation of the amplitude, width and achievable precisions. Each of these properties is determined from an individual column (i.e., cross-scan position, i.e., in-scan PSF). These models are for a star with $T_{eff} = 3,500$K. The two left-hand panels are for the wide astrometric band (400-900 nm), the two right-hand panels for the narrow astrometric band (550-850 nm). The astrometric and photometric accuracies depend on the total number of photo electrons and are copied from previous work (see text). The peak number of electrons in the top row is 100,000 electrons (2D full-well capacity). The accuracies are for a star 5 magnitudes (factor 100) brighter. The variation of the in-scan width (middle panels) is due to a change in mean wavelength with cross-scan position.

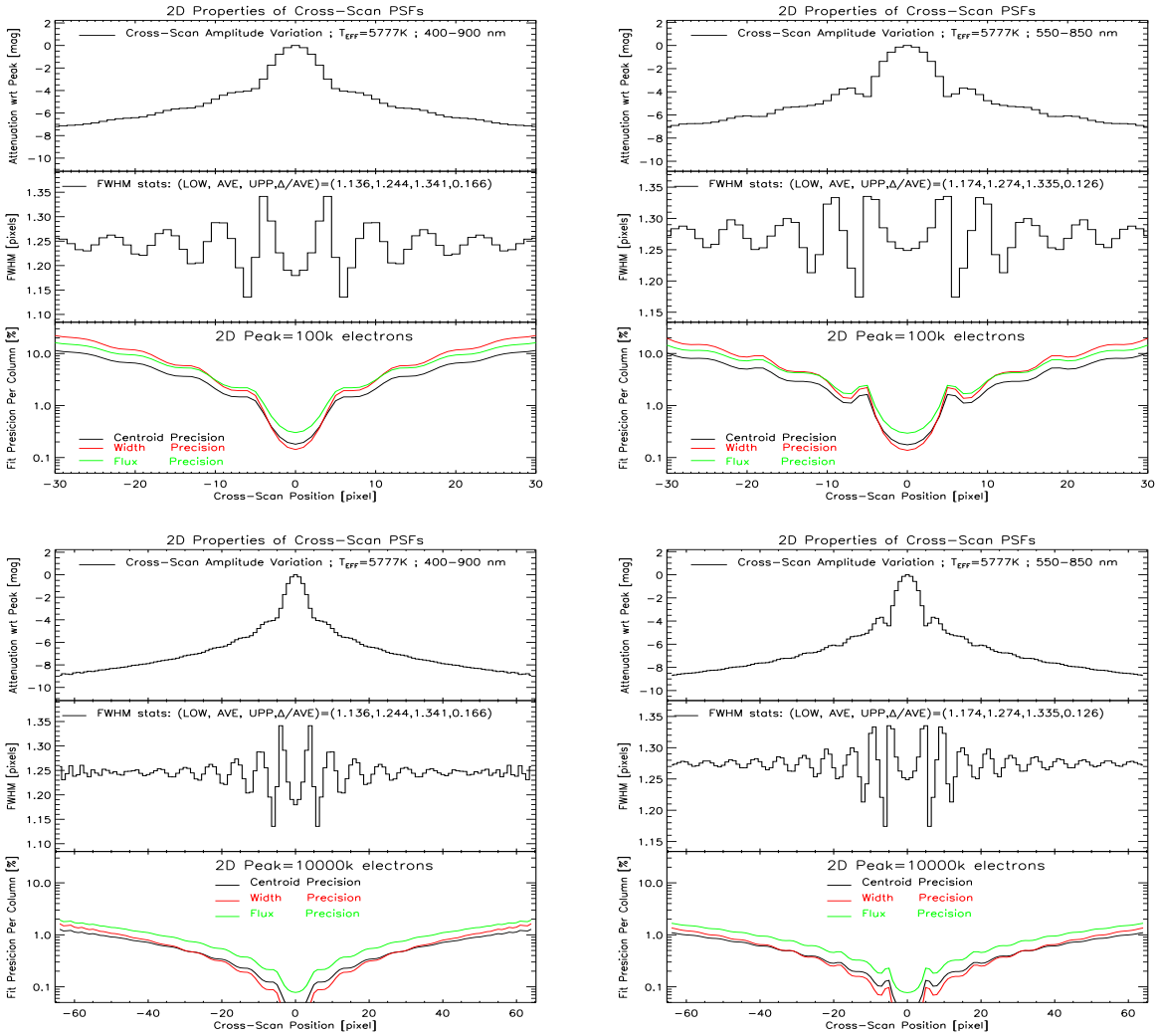

Fig. 3.— Same as figure 2 but for a Solar-type star.

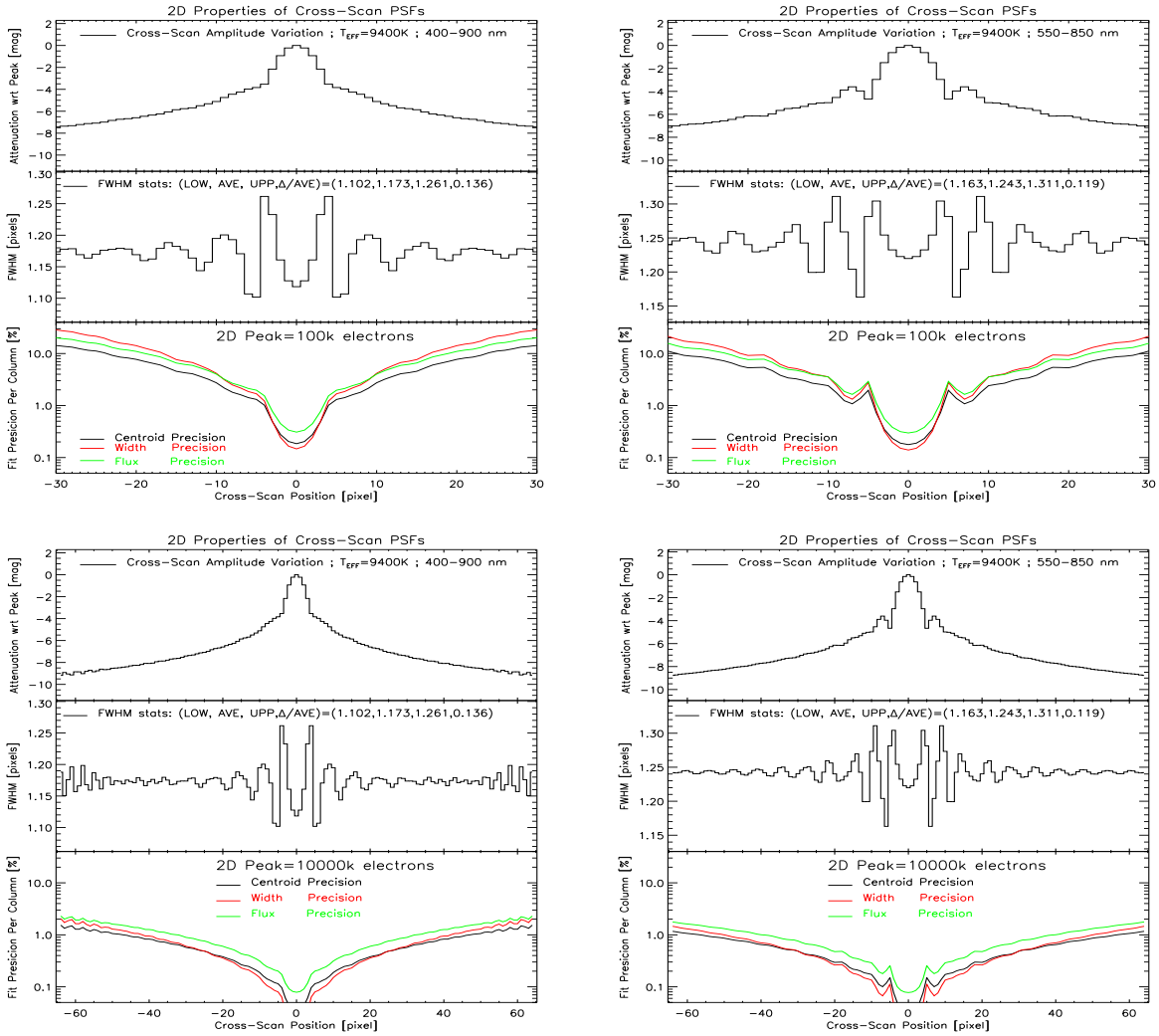

Fig. 4.— Same as figure 2 but for a Vega-like star.

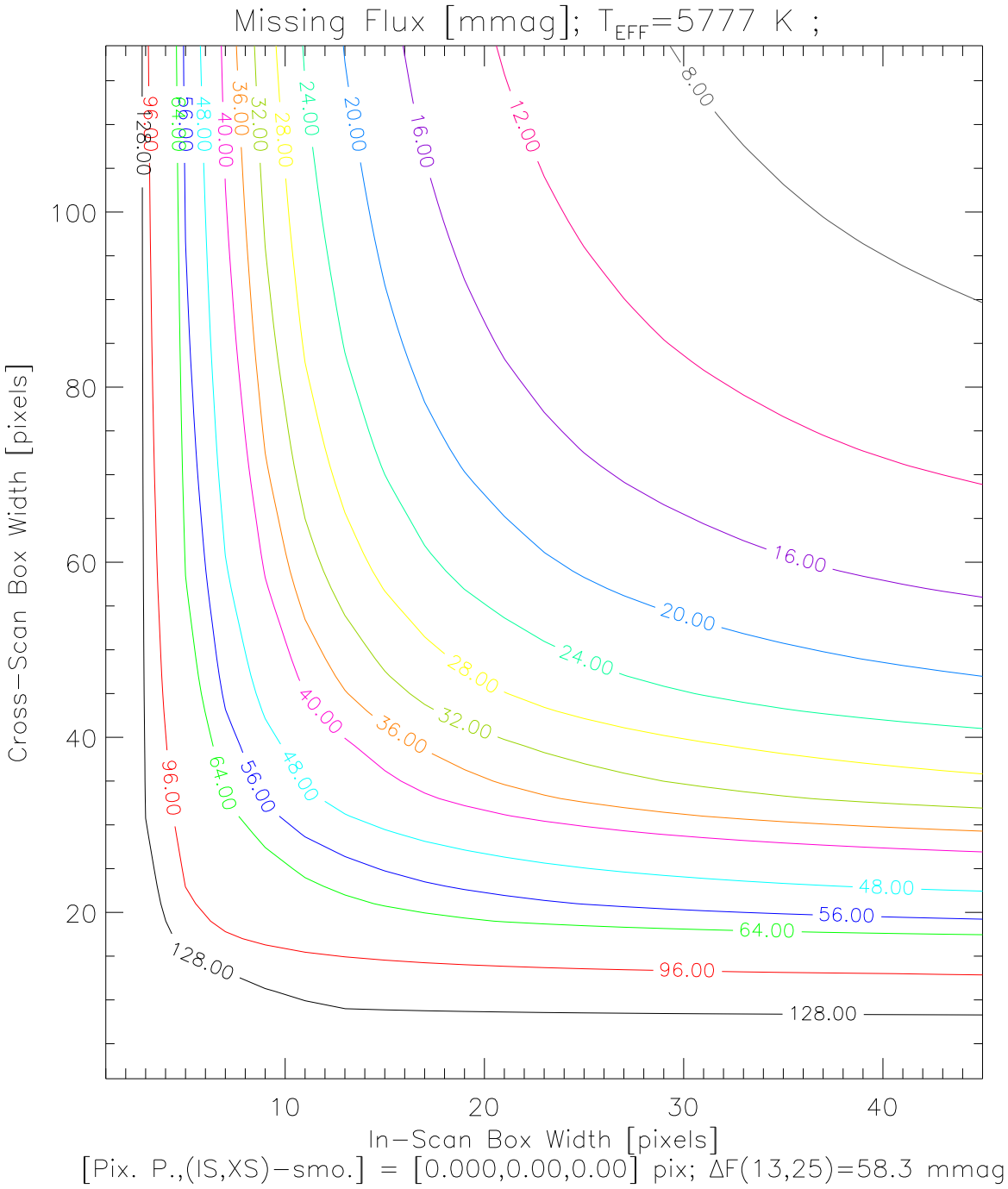

Fig. 5.— The fraction of the total flux (in mmag) that falls outside the "box." The in-scan and cross-scan box size can be read off from the abscissa and ordinate, respectively. This model was generated for a Solar-type star and the narrow astrometric bandpass.

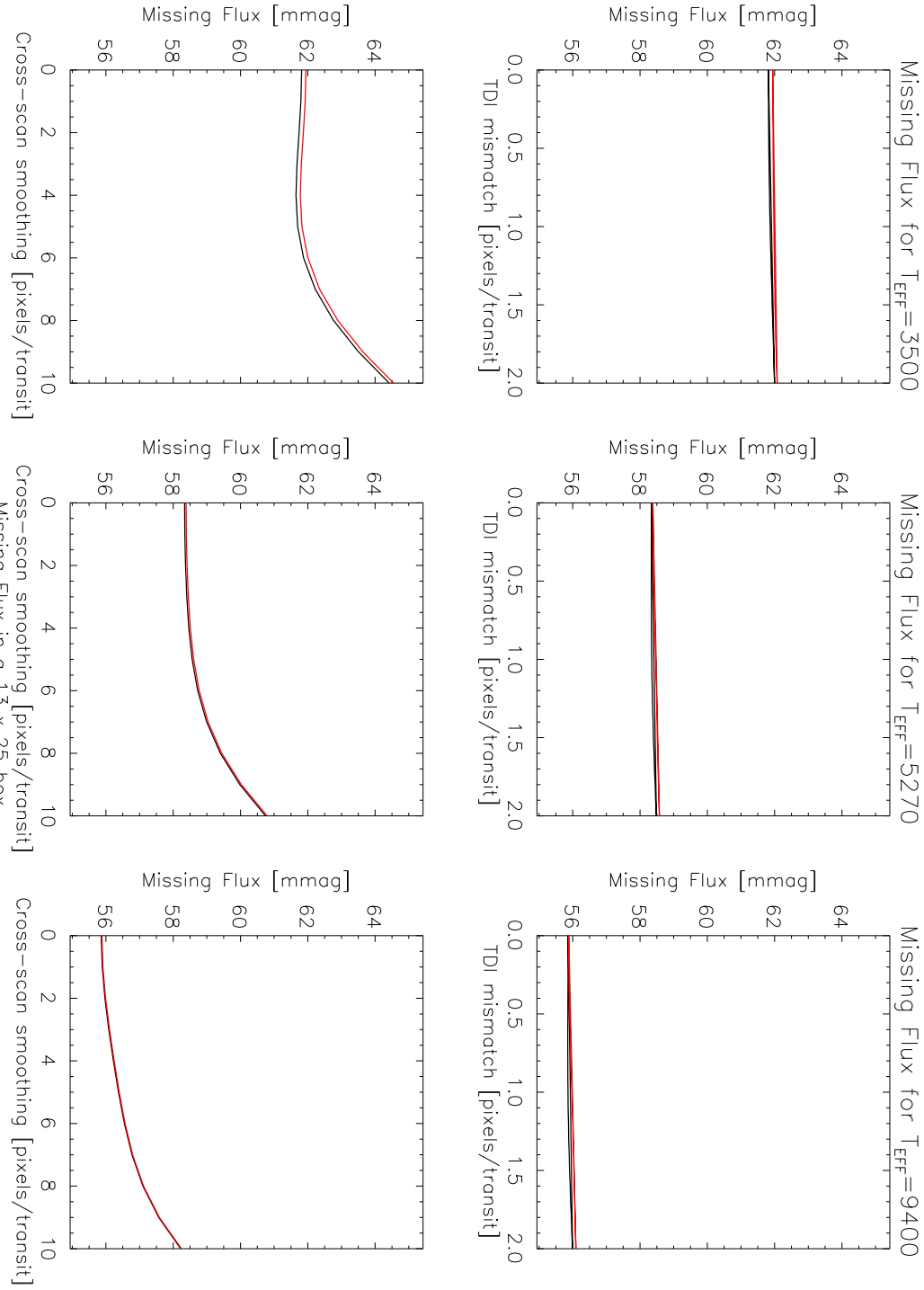

Fig. 6.— The fraction of the total flux that falls outside the "box," as a function of TDI mismatch rate (top panels) and cross-scan smearing (bottom panels). The three columns were calculated for T_{eff} =3,500, 5,777 and 9,400 K, from left to right, respectively. The two lines in each plot are for the wide and narrow passband. The amount of missing flux depends strongly upon spectral type, but only weakly on TDI mismatch and cross-scan rate.